Ceramics International 44 (2018) 10551–10557

Contents lists available at ScienceDirect

Ceramics International

journal homepage: www.elsevier.com/locate/ceramint

Effect of Sr^{2+} and Ba^{2+} doping on structural stability and mechanical properties of $La_2NiO_{4+\delta}$

A. Akbari-Fakhrabadi[a,*], E.G. Toledo[a], J.I. Canales[a], V. Meruane[a], S.H. Chan[b], M.A. Gracia-Pinilla[c,d]

[a] Advanced Materials Laboratory, Department of Mechanical Engineering, University of Chile, Santiago, Chile
[b] Energy Research Institute, School of Mechanical and Aerospace Engineering, Nanyang Technological University, Singapore
[c] Universidad Autónoma de Nuevo León, Facultad de Ciencias Físico-Matemáticas, Av. Universidad, Cd. Universitaria, San Nicolás de los Garza, N.L., Mexico
[d] Universidad Autónoma de Nuevo León, Centro de Investigación e Innovación en Desarrollo de Ingeniería y Tecnología, PIITKm6, Carretera al Aeropuerto, Apodaca, N.L., Mexico

ARTICLE INFO

Keywords:
Lanthanum Nickelate
$La_{1.8}Sr_{0.2}NiO_{4+d}$
$La_{1.8}Ba_{0.2}NiO_{4+d}$
Structure
Mechanical properties

ABSTRACT

Structural and mechanical Characterizations of $La_{1.8}M_{0.2}NiO_{4+\delta}$ (M: Sr and Ba) prepared by low frequency ultrasound assisted synthesis technique and sintered at different temperatures were studied. HRTEM and XRD analyses showed the uniform shape of calcined nanocrystalline powders with the particle size of less than 100 nm with mixed phases, which were refined by Rietveld method using orthorhombic (Fmmm) and tetragonal (F4/mmm) structures. Sintering $La_{1.8}Sr_{0.2}NiO_{4+\delta}$ and $La_{1.8}Ba_{0.2}NiO_{4+\delta}$ compacted discs at temperatures higher than 1300 °C and 1250 °C, respectively, resulted in appearance of extra peaks close to a monoclinic phase. Doping $La_2NiO_{4+\delta}$ with Sr^{2+} and Ba^{2+} did not affect its sinterability and average grain size significantly, however, Ba^{2+} improved the elastic modulus and microhardness, while Sr^{2+} improved the fracture toughness.

1. Introduction

Lanthanum-based mixed oxides such as $La_{1-x}Sr_xCo_yFe_{1-y}O_{3-d}$ (LSCF) and $La_2NiO_{4+\delta}$ (LNO) are attractive mixed ionic and electronic conductive (MIEC) materials for oxygen electrode of solid oxide cells [1] and ceramic oxygen ion transport membrane for producing oxygen [2] due to their good catalytic activity for oxygen reduction reactions. In recent years, lowering the operating temperature of such devices is the focus of many studies for their greater economic feasibility and long-term reliability. To promote the relatively slow oxygen reduction reaction kinetics when lowering the operating temperature, LNO has been introduced as a promising alternative, which shows a smaller coefficient of thermal expansion and a better chemical stability under working conditions [3,4]. LNO is a perovskite-derived K_2NiF_4 type oxide constructed alternatively with $LaNiO_3$ and La_2O_2 layers along c-axis direction [5,6], where it exhibits unique properties such as high oxygen permeation flux for oxygen ion transportation by a combination of vacancy diffusion in the perovskite layer and interstitial sites between the rock-salt and perovskite layers [7,8]. However, the electrical conductivity of LNO is not sufficient as a cathode material under the intermediate operating temperatures [4]. Similar to LSCF, doping La^{3+} site with alkaline earth ions in LNO such as Sr^{2+} or Ba^{2+} improves its electrical conductivity by generating extra electron holes for charge compensation [9–12]. Although, many studies have concentrated on the effect of dopants on structural, conduction properties and electrochemical behavior of LNO, their associated mechanical properties studies are limited in the literature; only thermo-mechanical properties of porous LNO [13] and mechanical properties of aqueous tape cast LNO membranes [14] are available.

As the knowledge of mechanical properties of these materials is essential to determine the lifespan of the above-mentioned devices and an indication of their reliability [15], effect of Sr^{2+} and Ba^{2+} doping on structure stability and mechanical properties of LNO are investigated thoroughly in this paper.

2. Experimental

To prepare $La_2NiO_{4+\delta}$ (LNO), $La_{1.8}Sr_{0.2}NiO_{4+\delta}$ (LSNO) and $La_{1.8}Ba_{0.2}NiO_{4+\delta}$ (LBNO), appropriate amounts of $La(NO_3)_3$-$6H_2O$, $Ni(NO_3)_3$-$6H_2O$, $Sr(NO_3)_2$ and $Ba(NO_3)_2$ (Sigma-Aldrich, 99.9%) precursors were dissolved in distilled water by a magnetic stirrer. Then the precursor solution under vigorous mechanical stirring was irradiated in an ultrasonic bath (~50 kHz) and NaOH solution (20%) was added drop-wise to maintain the pH of the solution during the synthesis and it

* Corresponding author.
E-mail address: aliakbarif@ing.uchile.cl (A. Akbari-Fakhrabadi).

https://doi.org/10.1016/j.ceramint.2018.03.077
Received 2 January 2018; Received in revised form 8 March 2018; Accepted 10 March 2018
Available online 13 March 2018

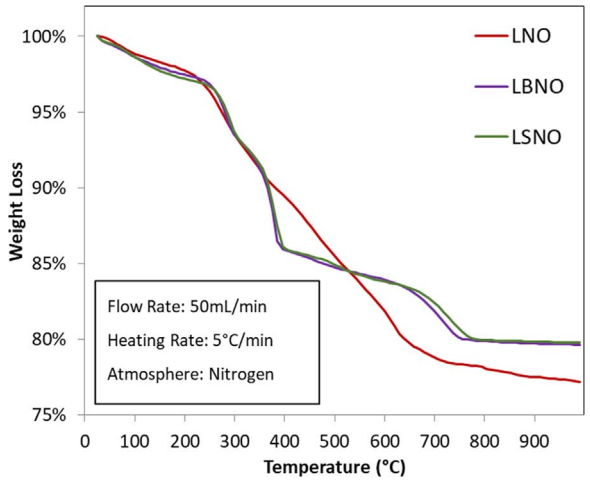

Fig. 1. Thermogravimetric analysis curve of as dried (110 °C/24 h) nanomaterials.

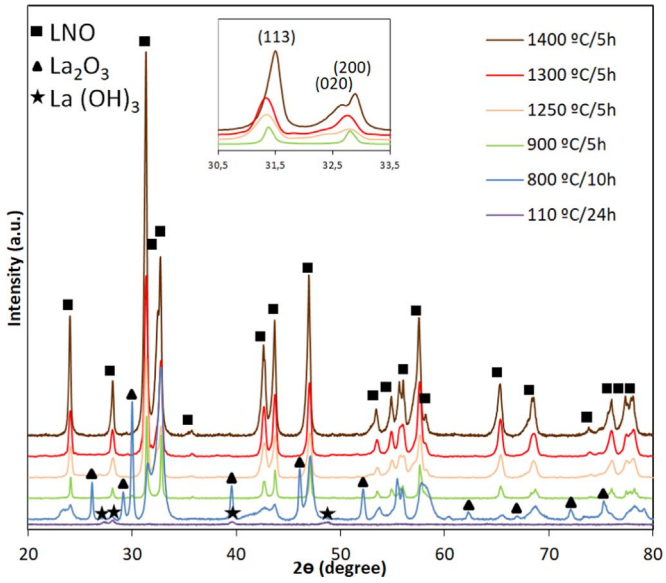

Fig. 2. XRD patterns of as dried (110 °C/24 h), calcined (800 °C/10 h and 900 °C/5 h) LNO nanopowders and sintered discs (1250, 1300 and 1400 °C/5 h).

was kept under stirring and irradiation for one hour. Subsequently, the obtained materials were filtered, re-dispersed and washed with distilled water for several times until reaching the neutral pH, dried at 110 °C for 24 h and then calcined at 900 °C for 5 h. The thermogravimetric (TG) analysis of the as-dried materials was performed using Netzsch TG 209 F1 Libra.

The morphology, particle size and structure of calcined nanopowders were characterized by XRD (Bruker D8) and TEM (Tecnai F20 FEG and FEI TITAN G2 80-300). Rietveld refinement of the XRD patterns was done using TOPAS 4.2 software.

The calcined powder was then uniaxially pressed (90 MPa) to form green discs (D = 25 and t = 3 mm), which were subsequently sintered at temperatures between 1250 and 1400 °C for 5 h. The surface of sintered discs was polished and thermally etched at 50 °C lower than the sintering temperature for 30 min. Heating and cooling rate for sintering and thermal etching are maintained at 60 °C/h and 30 °C/h, respectively, for all samples. The average grain sizes were obtained by measuring diameters of more than 500 grains from the scanning electron

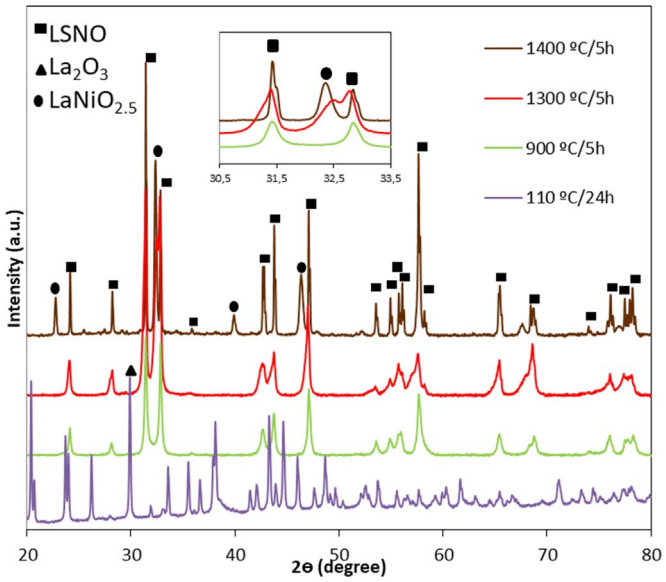

Fig. 3. XRD patterns of as dried (110 °C/24 h), calcined (900 °C/5 h) LSNO nanopowders and sintered discs (1300 and 1400 °C/5 h).

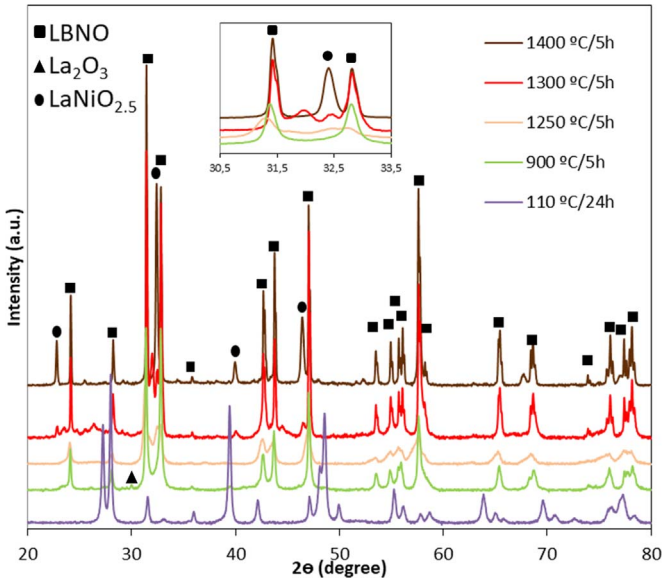

Fig. 4. XRD patterns of as dried (110 °C/24 h), calcined (900 °C/5 h) LBNO nanopowders and sintered discs (1250, 1300 and 1400 °C/5 h).

microscopy (SEM) micrographs. The structural characteristics of sintered discs were analysed by XRD with the same equipment. The Young's moduli of sintered discs were determined using the impulse excitation technique (IET). The details of the method have been reported elsewhere [16]. The micro-hardness of the sintered discs was determined using Vikers microhardness tester (Struers). At least 15 indentations per load were performed for a dwelling time of 15 s. The indentation fracture toughness (K_{IC}) was calculated by direct measurements of the crack lengths using SEM.

3. Results and discussion

The TG curves of the as-dried materials are illustrated in Fig. 1. The

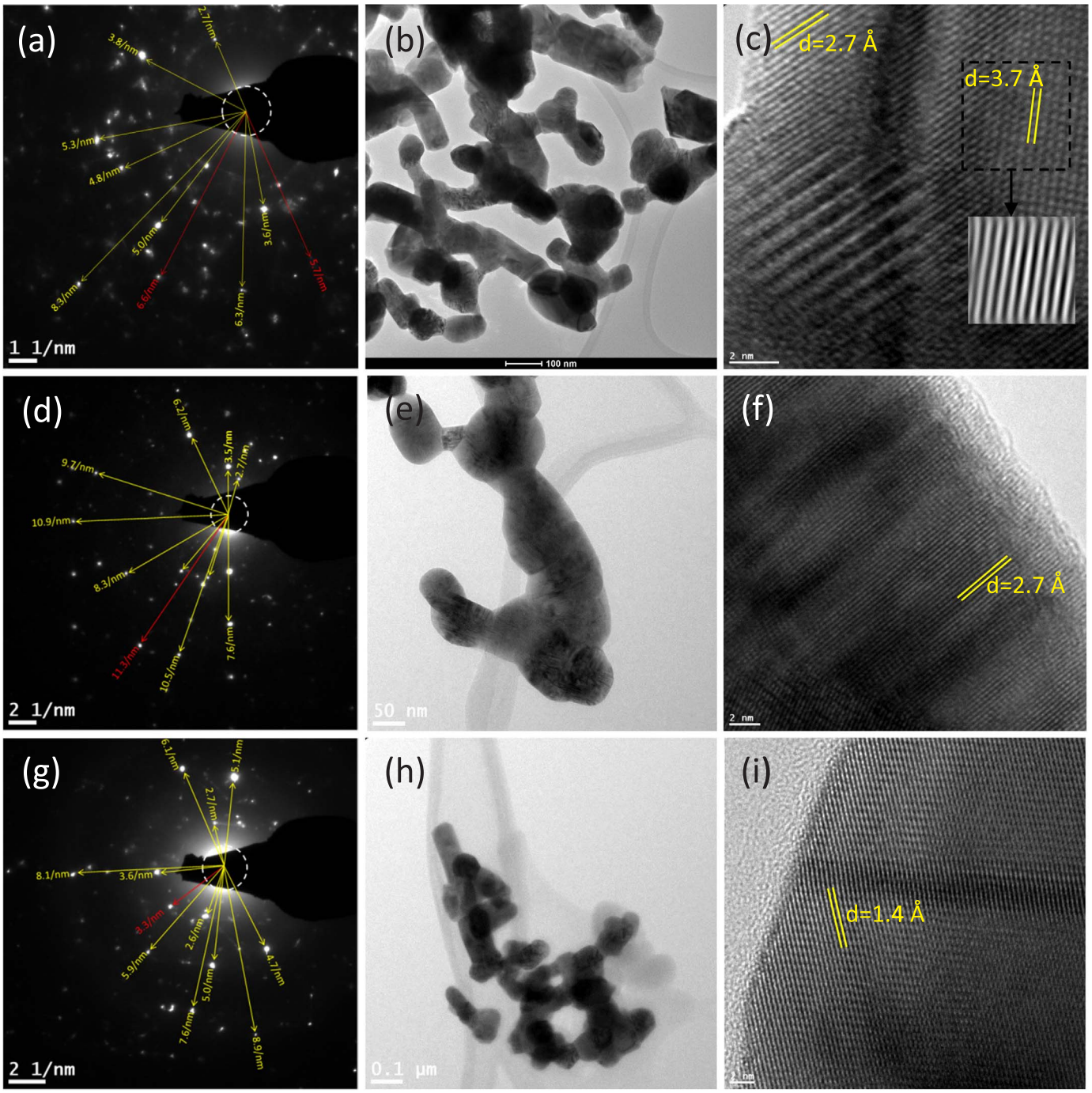

Fig. 5. HRTEM micrographs and SAED patterns of (a, b, c) LNO, (d, e, f) LSNO and (g, h, i) LBNO nanopowders calcined at 900 °C/5 h. (For interpretation of the references to color in this figure legend, the reader is referred to the web version of this article.)

three similar steps in all compounds were detected. The first weight loss occurred at temperatures up to 200 °C, where the bound water was removed. The second steps of weight loss of about 18% were observed between 200 and 700 °C where the decomposition of metal hydroxides and carbonates take place [17]. The third observed weight loss of about 1% is attributed to the decomposition of La_2O_3 and crystal growth to form Ruddlesden–Popper nanostructures.

Figs. 2, 3 and 4 show XRD patterns of as-dried, calcined and sintered pellets of LNO, LSNO and LBNO, respectively. The XRD patterns of as-dried precursors show the peaks corresponding to related metal hydroxides such as $La(OH)_3$ (JCPDS # 36-1481) and $Ni(OH)_2$ (JCPDS # 14-0117); based on which the main reactions involved during the sonication can be written as:

$$2La(NO_3)_3\text{-}6H_2O + Ni(NO_3)_2\text{-}6H_2O + 8NaOH \rightarrow 2La(OH)_3 + Ni(OH)_2 + 8NaNO_3 + 18H_2O$$

As it can be seen, calcination of LNO precursor at 800 °C/10 h shows the peaks corresponding to La_2O_3 and perovskite-derived K_2NiF_4 type nanostructures. With increasing calcination temperature to 900 °C/5 h, the amount of La_2O_3 as impurity was decreased, which confirms TG

Table1
The structure parameters and XRD refinement results of LNO nanopowders calcined at 900 °C/5 h.

Space group	Fmmm	I4/mmm
a (Å)	5.4628	3.9011
b (Å)	5.4611	
c (Å)	12.6944	12.3124
Crystal size (nm)	96	22
La	0.3605, 1, 0.1244	0.3766, 1, 3.887
z/c, Occ., Beq		
O(1)	0.9706, 2.88	0.01, 4
Occ., Beq		
O(2)	0.2033, 0.3199, 2	0.2055, 1, 4
z/c, Occ., Beq		
O(3)	− 0.0005, 0.0575, 0.1612	− 0.14165, 0.8997, 0.0000
x/a, y/b, z/c		
Occ., Beq	0.1621, − 2	0.5757, − 3
O(4)	0.1337, 0.0887, − 3	0.25, 1, − 1.307
z/c, Occ., Beq		
R (Bragg)	0.616	1.564
wt%	94	5
Impurities (wt%)	La_2O_3 (~1)	
R_{exp} (%)	3.63	
R_{wp} (%)	4.84	
R_p (%)	3.85	
GOF	1.33	

Table 2
The structure parameters and XRD refinement results of LSNO nanopowders calcined at 900 °C/5 h.

Space group	Fmmm	I4/mmm
a (Å)	5.4621	3.8776
b (Å)	5.4557	
c (Å)	12.7076	12.5001
Crystal size (nm)	88	103
La/Sr	0.3611, 0.8/0.03, − 3.158/	0.3456, 1/0.36, 1.573/
z/c, Occ., Beq	− 5	0.884
O(1)	1, 5	1, − 5
Occ., Beq		
O(2)	0.1705, 0.8394, − 5	0.1813, 1, − 5
z/c, Occ., Beq		
O(3)	− 0.5027, − 0.1792, 0.1532	0.0665, 0.0664, − 0.0145
x/a, y/b, z/c		
Occ., Beq	0.1652, − 6.638	1, − 5
O(4)	0.2132, 0.2235, 5	0.25, 1, 5
z/c, Occ., Beq		
R (Bragg)	0.786	2.241
wt%	84	15.9
Impurities (wt%)	La_2O_3 (~0.1)	
R_{exp} (%)	2.66	
R_{wp} (%)	4.79	
R_p (%)	3.66	
GOF	1.8	

results as mentioned above. Fig. 5 shows HRTEM micrographs of the calcined LNO, LSNO and LBNO nanocrystaline particles with an average particle size of ~100 nm and clear internal crystal lattice structures, which confirm the high crystallinity and are in good agreement with the XRD results. As it can be seen in Figs. 5a, 5d and 5g, selected area electron diffraction (SAED) images confirmed the electron diffractions of Ruddlesden–Popper nanostructures (yellow) and La_2O_3 (red). The measurement accuracy has limited the identification of respective planes in each phase. The alternatively arranged perovskite and rock-salt layered structure of $La_{2-x}M_xNiO_{4+d}$ (M: Sr and Ba) has been reported with orthorhombic (Fmmm and Bmab) and tetragonal (F4/mmm and P42/ncm) crystal structures and the mixed phases are dependent on oxygen and dopants concentration and distribution [18,19]. The room temperature XRD patterns of nanopowders calcined at 900 °C/5 h were refined by Rietveld method using the above- mentioned four models, among whose mixed structures of Fmmm and F4/mmm had been reported by Aguadero et al. [20] with pseudo Voigt peak shape showed the best obtained fit between the calculated and experimental XRD profiles. The obtained structural parameters are summarized in Tables 1, 2 and 3 for LNO, LSNO and LBNO, respectively. As it can be seen, Fmmm structure has weight percent majority in the three compositions, however, adding Sr and Ba dopants would increase the amount of F4/mmm phase, in which a unit-cell parameter decreases, while c increases with increasing ionic size of dopants [12]. Comparing occupying factors for La and dopants in both phases shows the segregation of dopants to F4/mmm domains. XRD patterns of fired LNO pellets at temperatures up to 1400 °C, as illustrated in Fig. 2, shows decomposition of La_2O_3 and split of (020)/(200) reflections, which is considered as orthorhombic phase manifestation as h‡k in this structure. XRD patterns of LSNO (Fig. 3) and LBNO (Fig. 4) sintered discs up to 1300 °C and 1250 °C, respectively, show the same reflections as LNO sintered discs, however, sintering at temperatures higher than above

Table 3
The structure parameters and XRD refinement results of LBNO nanopowders calcined at 900 °C/5 h.

Space group	Fmmm	I4/mmm
a (Å)	5.4694	3.8619
b (Å)	5.4555	
c (Å)	12.7040	12.5572
Crystal size (nm)	96	12.5
La/Ba	0.3619, 0.91/0.1, − 0.92/	0.3545, 0.7/0.3, − 2.397/
z/c, Occ., Beq	2.27	− 2.632
O(1)	1, 2.995	1, − 2.667
Occ., Beq		
O(2)	0.1905, 0.79, 2.04	0.1659, 1, − 2,75
z/c, Occ., Beq		
O(3)	− 0.0921, − 0.0402,	0.01663, − 0.07759, 0.0858
x/a, y/b, z/c	0.4201	
Occ., Beq	0.1992, − 2	1, 1.381
O(4)	0.2508, 0.099, 1.953	0.25, 1, 3.75
z/c, Occ., Beq		
R (Bragg)	1.423	1.758
wt%	83	16.7
Impurities (wt%)	La_2O_3 (~0.3)	
R_{exp} (%)	2.13	
R_{wp} (%)	5.90	
R_p (%)	4.24	
GOF	2.78	

Table 4
Average grain size, densities and elastic modulus of LNO, LSNO and LBNO discs sintered at different temperatures for 5 h.

	Sintering temperature (°C)	Average grain size (μm)	Measured density (g cm^{-3})	Elastic modulus (GPa)
LNO	1250	0.79	6.3	132.7
	1300	1.45	6.6	146.0
	1400	4.2	6.9	152.8
LSNO	1300	1.4	6.3	147.0
LBNO	1250	0.87	6.2	147.8

mentioned would result in decomposition of LSNO and LMNO to K_2NiF_4 and monoclinic (JCPDS # 049-1011) structures as its reflections can be seen in Figs. 3 and 4. The bimodal phase mixtures and phase separation in $La_{2-x}Sr_xNiO_{4+\delta}$ structure containing Sr with level x > 0.5 values having Sr-poor and Sr-rich phases have been reported in literature [18,20–22] and attributed to synthesis condition and equilibrium immiscibility at the final temperature of processing due to inhomogeneous distribution of A cations within the specimen. Observation of phase separation in $La_{2-x}M_xNiO_{4+\delta}$ (M: Sr and Ba) indicates that there may be relationship with synthesis method, sintering profile and post annealing conditions, which affect La/M-dopant distributions within the samples with changing oxygen content of each phase due to reducing the positive net charge in rocksalt layer and negative net charge in the NiO_2 planes [18].

Table 4 tabulates the average grain size, measured density and elastic modulus of LNO, LSNO and LBNO discs sintered at different temperatures for 5 h, which show that average grain size and density of LNO discs increased with increasing sintering temperature. However, doping with Sr^{2+} and Ba^{2+} did not affect these properties of LNO, significantly. Elastic modulus of LNO increased with increasing temperature, which can be related to decreasing porosity with sintering at higher temperatures and E = 152.8 GPa for disc sintered at 1400 °C/5 h is close to that reported by Huang et al. determined by 4-point bending test [13]. Although, doping LNO with Sr^{2+} did not affect elastic modulus, the elastic modulus of LBNO shows higher value than that of LNO for discs sintered at the same temperatures. Having higher elastic modulus doped LNO discs with similar measured density may be

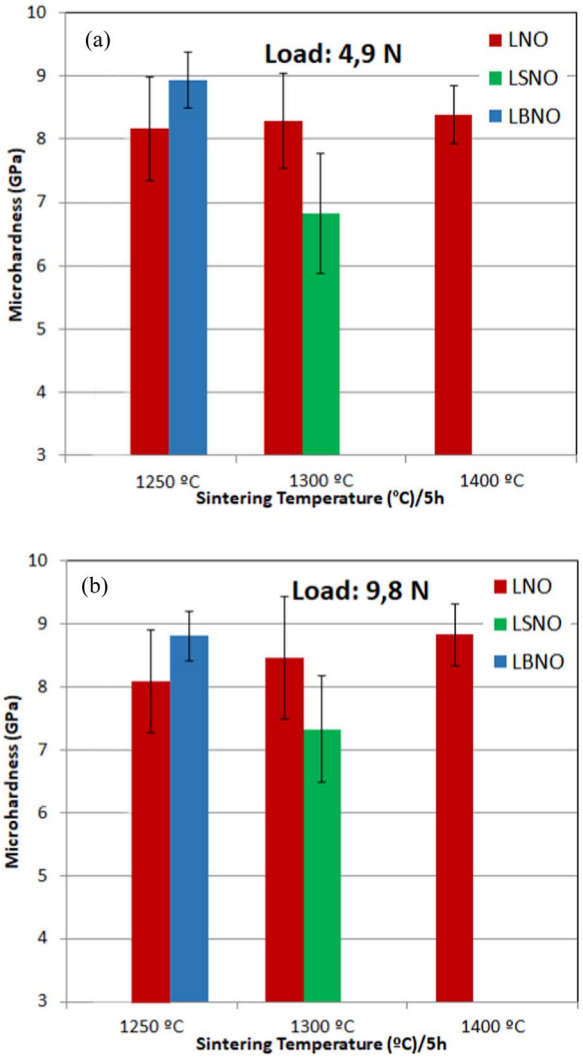

Fig. 6. Microhardness of LNO, LSNO and LMNO discs sintered at different temperatures for applied loads of (a) 4.9 N and (b) 9.8 N.

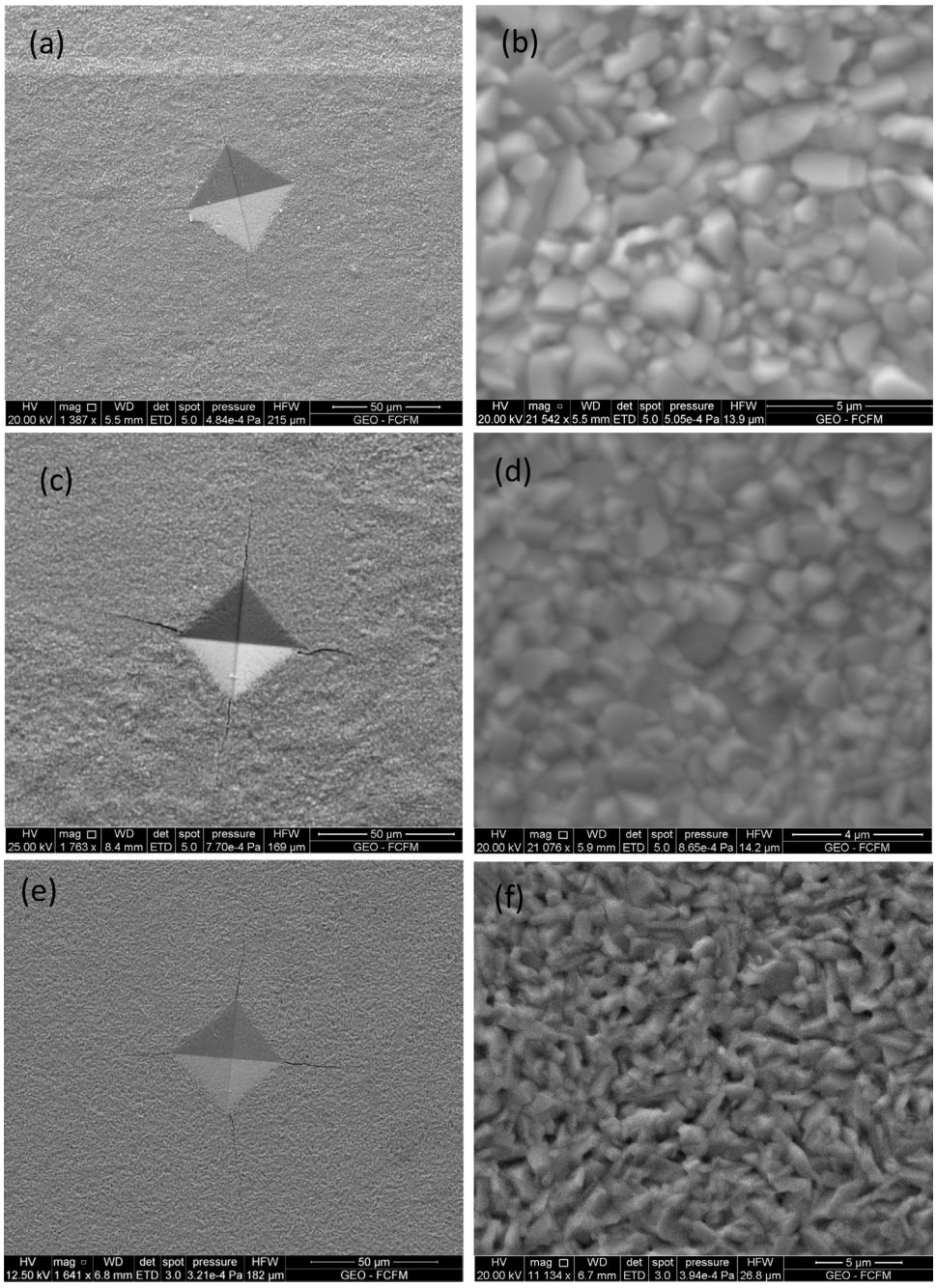

Fig. 7. Vickers indentation marks and SEM micrographs of thermally etched (1200 °C/30 min) (a, b) LNO, (c,d) LSNO and (e, f) LBNO discs sintered at 1250 °C/5 h.

attributed to relief of the tensile stress in the La–O bonds due to doping of La^{3+} with larger Sr^{2+} and Ba^{2+} [12].

Microhardness of LNO, LSNO and LBNO discs sintered at different temperatures were measured by applying two different loads of 4.903 and 9.807 N after thermal etching. As shown in Fig. 6, obtained hardness are comparable to the hardness of LNO pellet with similar grain size but different applied load of 1.96 N [14]. As it can be seen, microhardness of LBNO is higher, while LSNO is lower than those of LNO in similar sintering temperatures. As it can be seen in Fig. 7, the transgranular cracks observed near the indents, which were used to calculate the fracture toughness as a function of these cracks sizes using Anstis's [23] formula. The calculated fracture toughness presented in Fig. 8 shows lower values for LNO compared with those reported by Chen et al. [14]. As it can be seen, LNO fracture toughness decreased with increasing sintering temperature, which is related to bigger average grain size obtained with sintering at higher temperature and is similar to that reported by Chen et al. [14]. Doping with Sr^{2+} and Ba^{2+} affects the fracture toughness, hence LSNO has exhibited the highest fracture toughness compared with LNO and LBNO discs sintered at different temperatures.

4. Conclusion

Using low frequency ultrasound (50 kHz) assisted synthesis method to obtain $La_2NiO_{4+\delta}$, $La_{1.8}Sr_{0.2}NiO_{4+\delta}$ and $La_{1.8}Ba_{0.2}NiO_{4+\delta}$ resulted in nanocrystalline orthorhombic and tetragonal mixed structures after

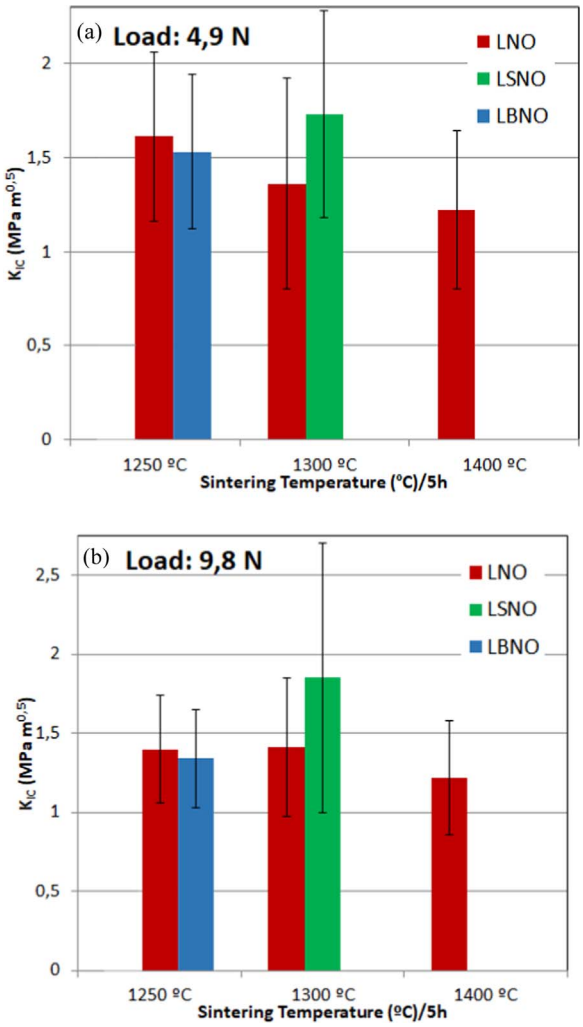

Fig. 8. Fracture toughness of LNO, LSNO and LMNO discs sintered at different temperatures for applied loads of (a) 4.9 N and (b) 9.8 N.

calcination of dried precursors at 900 °C/5 h. Densification of $La_{1.8}Sr_{0.2}NiO_{4+\delta}$ and $La_{1.8}Ba_{0.2}NiO_{4+\delta}$ at temperatures higher than 1300 °C and 1250 °C, respectively, showed their decompositions to K_2NiF_4 and monoclinic-like structures. The results of mechanical characterizations of E = 147.8 GPa and Hv = 8.9 GPa for LBNO and K_{IC} = 1.85 MPa $m^{0.5}$ for LSNO demonstrated that doping $La_2NiO_{4+\delta}$ with Ba^{2+} has improved its elastic modulus and microhardness, while Sr^{2+} doping has improved its fracture toughness.

Acknowledgements

The authors acknowledge FONDECYT, Government of Chile (Project No.: 11160202), for the support to carry out this project.

References

[1] S.Y. Gómez, D. Hotza, Sustain. Energy Rev. 61 (2016) 155–174.
[2] P.I. Dahl, M.L. Fontaine, F. Ahouanto, C. Denonville, O. Paulsen, Y. Larring, T. Peters, P.P. Henriksen, R. Bredesen, Energy Procedia 23 (2012) 187–196.
[3] W. Li, B. Guan, X. Zhang, J. Yan, Y. Zhou, X. Liu, Phys. Chem. Chem. Phys. 18 (2016) 8502–8511.
[4] Y.P. Wang, Q. Xu, D.P. Huang, K. Zhao, M. Chen, B.H. Kim, Int. J. Hydrog. Energy 41 (2016) 6476–6485.
[5] M. Matsuda, M. Hashimoto, C. Matsunaga, T.S. Suzuki, Y. Sakka, T. Uchikoshi, J. Eur. Ceram. Soc. 36 (2016) 4077–4082.
[6] C. Jeong, J.H. Lee, M. Park, J. Hong, H. Kim, J.W. Son, J.H. Lee, B.K. Kim, K.J. Yoon, J. Power Sources 297 (2015) 370–378.
[7] S.Y. Jeon, H.N. Im, B. Singh, J.H. wang, S.J. Song, Ceram. Int. 39 (2013) 3893–3899.
[8] S.Y. Gómez, J. Gurauskis, V. Øygarden, D. Hotza, T. Grande, K. Wiik, Solid State Ion. 292 (2016) 38–44.
[9] E. Boehm, J.M. Bassat, M.C. Steil, P. Dordor, F. Mauvy, J.C. Grenier, Solid State Sci. 5 (2003) 973–981.
[10] D.P. Huang, Q. Xu, F. Zhang, W. Chen, H.X. Liu, J. Zhou, Mater. Lett. 60 (2006) 1892–1895.
[11] A.A Kolchugin, E.Y. Pikalova, N.M. Bogdanovich, D.I. Bronin, S.M. Pikalov, S.V. Plaksin, M.V. Ananyev, V.A. Eremin, Solid State Ion. 288 (2016) 48–53.
[12] Y. Shen, H. Zhao, J. Xu, X. Zhang, K. Zheng, K. Swierczek, Int. J. Hydrog. Energy 39 (2014) 1023–1029.
[13] B.X. Huang, J. Malzbender, R.W. Steinbrech, Thermo-mechanical properties of $La_2NiO_{4+\delta}$, J. Mater. Sci. 46 (2011) 4937–4941.
[14] X. Chen, M.A. Einarsrud, T. Grande, J. Eur. Ceram. Soc. 35 (2015) 309–315.
[15] J. Fondard, A. Billard, G. Bertrand, P. Briois, Solid State Ion. 265 (2014) 73–79.
[16] A. Akbari-Fakhrabadi, V. Meruane, M. Jamshidijam, R.V. Mangalaraja, M.A. Gracia, Mater. Sci. Eng. A 649 (2016) 168–173.
[17] A. Akbari-Fakhrabadi, P. Sathishkumar, K. Ramam, R. Palma, R.V. Mangalaraja, Powder Technol. 276 (2015) 200–203.
[18] M. Hücker, K. Chung, M. Chand, T. Vogt, J.M. Tranquada, D.J. Buttrey, Phys. Rev. B 70 (2004) 1–10 (064105).
[19] J.D. Jorgensen, B. Dabrowski, Shiyou Pei, D.R. Richards, D.G. Hinks, Phys. Rev. B 40 (1989) 2187–2198.
[20] A. Aguadero, M.J. Escudero, M. Perez, J.A. Alonso, V. Pomjakushin, L. Daza, Roy. Soc. Ch 36 (2006) 4377–4383.
[21] J.E. Millburn, M.A. Green, D.A. Neumann, M.J. Rosseinsky, J. Solid State Chem. 145 (1999) 401–420.
[22] P.J. Heaney, A. Mehta, G. Sarosi, V.E. Lamberti, A. Navrotsky, Phys. Rev. B 57 (1998) 10370–10378.
[23] G.R. Anstis, P. Chantikul, B.R. Lawn, D.B. Marshall, J. Am. Ceram. Soc. 64 (1981) 539–543.